Nano Energy 83 (2021) 105832

Contents lists available at ScienceDirect

Nano Energy

journal homepage: http://www.elsevier.com/locate/nanoen

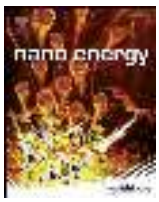

Communication

Evaluation and realization of safer Mg-S battery: The decisive role of the electrolyte

Lin Sheng [a,1], Zhangxiang Hao [a,1], Junrun Feng [a], Wenjia Du [c], Manxi Gong [a], Liqun Kang [a], Paul R. Shearing [c,d], Dan J.L. Brett [c], Yunhui Huang [b,*], Feng Ryan Wang [a,*]

[a] Materials and Catalysis Laboratory, Department of Chemical Engineering, University College London, Roberts Building, Torrington Place, London WC1E 7JE, UK
[b] State Key Laboratory of Materials Processing and Die & Mould Technology, School of Materials Science and Engineering, Huazhong University of Science and Technology, Wuhan 430074, China
[c] Electrochemical Innovation Lab, Department of Chemical Engineering, University College London, Roberts Building, Torrington Place, London WC1E 7JE, UK
[d] Harwell Science and Innovation Campus, Faraday Institution, Oxon, Didcot OX11 0RA, England, UK

ARTICLE INFO

Keywords:
Magnesium-sulfur battery
Electrolyte
Safety
Vapour pressure
Thermal runaway

ABSTRACT

The magnesium–sulfur (Mg-S) battery may be a safer alternative for the lithium-sulfur battery because Mg plating usually proceeds without dendrite formation. Here, we correlate the thermal runaway of Mg-S battery with the associated change of electrolyte vapour pressure via battery testing calorimetry. Over-pressure builds up along with the programmed heating of the cell, and as a result, the thermal runaway is triggered at 20–45 K over the electrolyte boiling point, corresponding to 70–150 kPa pressure difference between the cell and the environment. The distinct performance-safety-cost behaviours of three ether type of electrolytes stems from the different CH_2CH_2O chain lengths. Such molecular insight will serve as a fundamental guideline in choosing and designing the desired electrolyte that simultaneously achieves a high explosion limit and good electrochemical performance.

1. Introduction

Efficient and reversible energy storage is a driving force to enable consumer electronics, automotive propulsion, and to solve the intermittency of green electricity generation [1–5]. For domestic applications, a key requirement is to safely charge and discharge the battery at high energy densities [6,7]. One strategy to achieve high energy density is *via* the use of a Li-metal anode due to its specific capacity and low potential [8,9]. Upon cycling, metallic lithium forms needle-like dendrites, which impedes electrochemical performance over time and poses a fire hazard due to short circuit [10,11].

The magnesium-sulfur (Mg-S) battery is proposed to mitigate this safety concern as the production of magnesium dendrites is only seen at extreme condition with current density above 0.3 mA cm^{-2} [11–17]. Mg also has a high flash point, which is generally beyond the initial thermal runaway temperature of the battery. In addition, Mg is the fifth abundant element in the earth's crust [11,18], with a price 1/24 to that of lithium [19], and has a potential of − 2.37 V relative to SHE. The divalent Mg^{2+} enables two electrons transfer per Mg atom, providing a theoretical specific mass capacity of 2205 mAh g^{-1} and a specific volume capacity of 3832 mAh cm^{-3} [20–23]. While Mg-metal anode does not pose a potential risk due to the plating/stripping process [24–26], the thermal stability of the organic electrolytes that are employed in the Mg-S battery are a safety bottleneck of the whole system. So far, the thermal stability of the organic electrolytes and their safety concerns during battery operation are largely unknown [27–34]. A systematic methodology is required to perform battery safety evaluations and to identify the key descriptor to understand the physical and chemical changes of the electrolyte during thermal runaway [35–38]. Researchers have realized the importance of battery thermal safety and have carried out research, Xu *et al.* reported on the multi-level thermal safety of lithium batteries [39].

Here we evaluate the safety of three electrolytes by testing the Mg-S battery response to a controlled failure scenario, they are: 1,2-dimethoxyethane (DME), diglyme (DEG) and tetraglyme (TEG). The DME

* Corresponding authors.
E-mail addresses: huangyh@hust.edu.cn (Y. Huang), ryan.wang@ucl.ac.uk (F.R. Wang).
[1] These authors contributed equally to this work.

https://doi.org/10.1016/j.nanoen.2021.105832
Received 21 August 2020; Received in revised form 4 January 2021; Accepted 26 January 2021
Available online 28 January 2021

cell explodes at 403 ± 4 K (45 K above the boiling point) with corresponding vapour pressure of 249 ± 14 kPa. The DEG cell explodes at 455 ± 6 K (20 K above the boiling point) with corresponding vapour pressure of 172 ± 28 kPa. TEG has a higher boiling point, and thus the cell does not explode within the temperature range of the test. The result shows that the thermal runaway of the Mg-S batteries studied here is caused by the *in situ* heating and vaporization of the electrolyte, while the Mg anode and S cathode stay completely intact. Therefore, the vapour pressure of the electrolyte is the key descriptor of the overall battery safety. This conclusion suggests a potential way of optimizing battery safety and performance by molecular engineering new electrolyte systems with high ion conductivity and low vapour pressure.

2. Results and discussion

The overall evaluation of a battery electrolyte contains three criteria: electrochemical performance, safety, and cost (Fig. 1a). To study the electrolyte safety, the typical battery thermal runaway process needs to be simulated. It usually contains three stages [31]: 1: The onset of overheating in which the batteries arrive in an abnormal state with an increase of internal temperature; 2: Gasification of the electrolyte as the result of the heat accumulation. 3: Combustion and explosion of flammable electrolytes. To simulate this process, a programmed temperature profile is applied to the Mg-S coin cell at a given heating rate, while the temperature of the cell is monitored *in situ* in a battery testing calorimeter (BTC) (Fig. 1d and Fig. S1, Supporting Information). Such programmed temperature profile simulate heat generation when a cell undergoes a hard internal-short circuit (Stage 1) (Fig. 1f). As the temperature increases, the accumulated heat within the cell vaporizes the organic electrolytes (Stage 2), and eventually explosion occurs due to the over-pressure combustion (Stage 3). Such explosion will introduce a positive or negative temperature jump (TJ) in the temperature profile (Fig. 1d and e) due to the heat exchange between the cell and the environment. The explosion can destroy or deform the cell and the electrodes/separator layers will be scattered within the testing chamber (Fig. 1b and c). The objective of this study is to gain molecular insight into the structure derived explosion behaviours of the electrolyte in Mg-S battery.

DME, DEG and TEG are selected as the target electrolytes for the performance, safety and cost evaluation. They are linearly shaped ethers in the form of $CH_3O(CH_2CH_2O)_nCH_3$ with n equal to 1, 2 and 4, respectively. All of them reach the initial discharge capacity of 800 mAh g^{-1} (Fig. 2), while the first charge capacities are 800, 717 and 328 mAh g^{-1} for DME, DEG and TEG-cells, respectively. After three cycles the specific discharge capacities of DEG and TEG-cells are 61% and 46% of DME-cell (491 mAh g^{-1}). In addition, the discharge plateaus of DME and DEG-cells are at 1.0 V while that for TEG-cell is at 0.9 V. Such a difference in specific capacity stems from the number of CH_2CH_2O groups in the molecular structure. A longer molecule leads to reduced mobility of the electrolyte and thus higher resistance towards Mg^{2+} transportation [23,40]. As a result, the Mg^{2+} diffusion towards the CMK-3/S cathode is limited, causing insufficient charging and discharging.

Firstly, the fresh cells are tested in the BTC: a steady and linear temperature increase is found for all three cells during heating (Fig. 3a). Unlike the profile in conventional Li-ion batteries [37,41–43], here no significant heat generation is found in the form of sharp temperature spike, which suggests that combustion of Mg anode does not take place. Careful examination of all three curves reveals small TJ for DME and DEG-cells at 400 K and 450 K, respectively, indicating the explosion of the cell (Fig. 3b). In comparison, no TJ is found for the TEG-cell. Indeed, the DME-cell is completely destroyed during explosion, in which all six

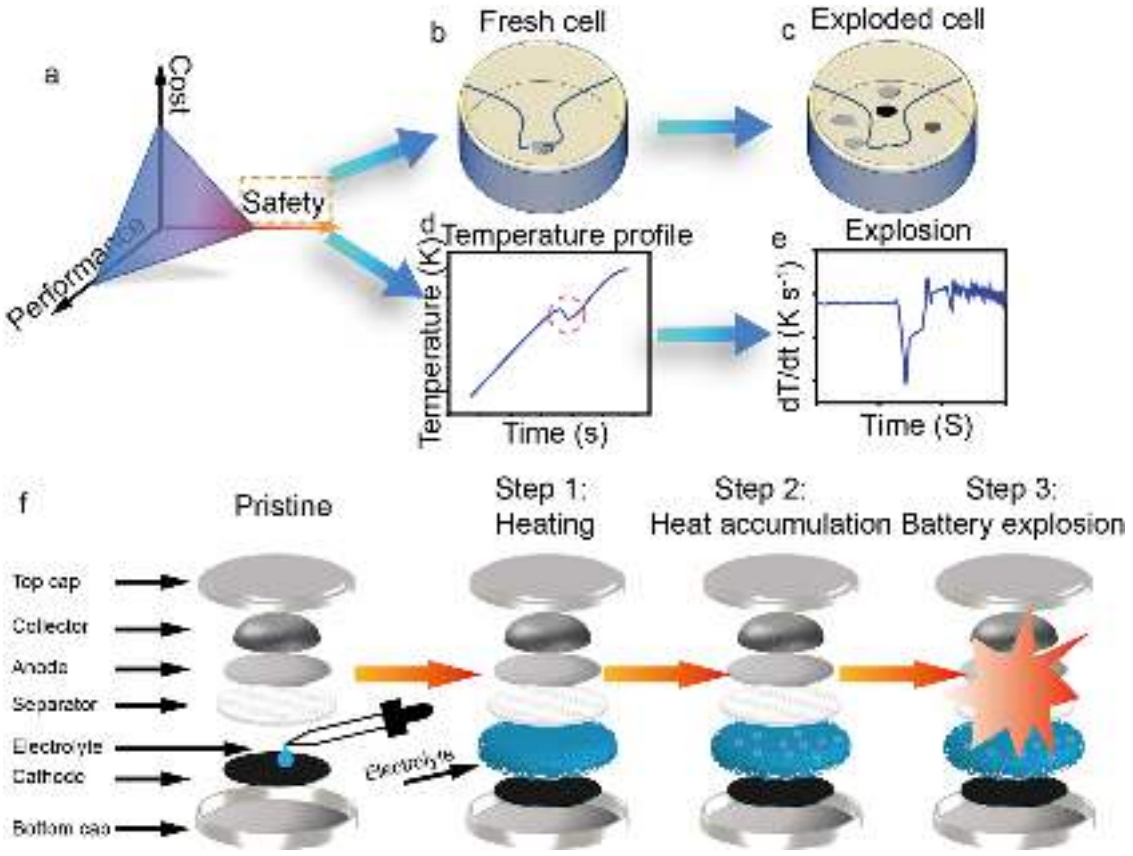

Fig. 1. (a) Three criteria for battery evaluation. (b, c) Schematic diagram before and after coin cells thermal runaway test. (d) Coin cells temperature change during thermal runaway test and (e) the first-order derivative of (d). (f) Schematic of three battery stages in the explosion test.

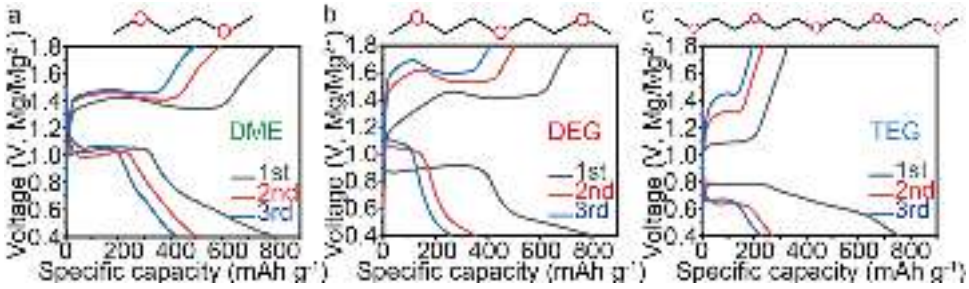

Fig. 2. (a)–(c) Charge and discharge curve of DME cell, DEG cell and TEG cell respectively.

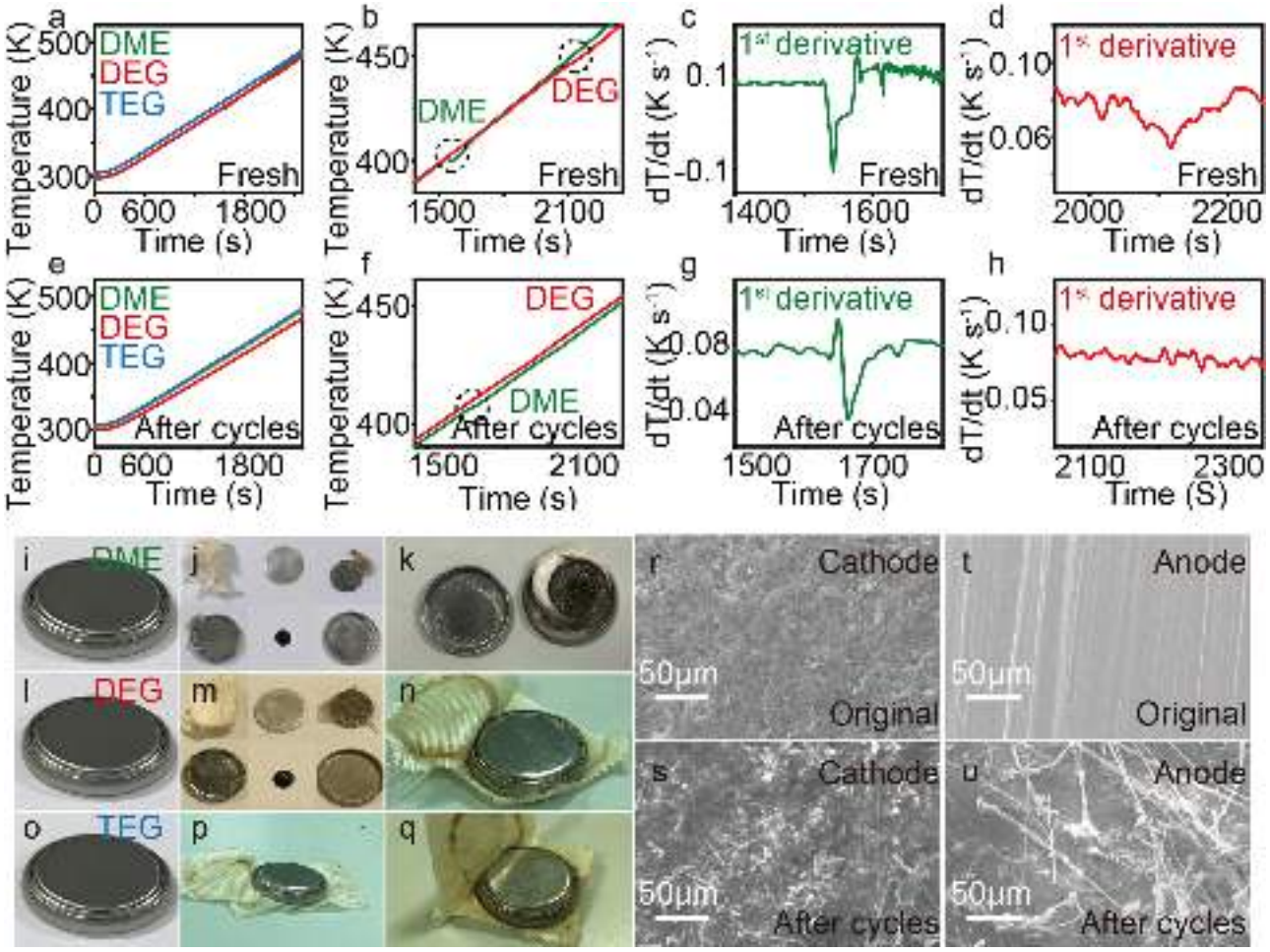

Fig. 3. (a,e) Temperature profile during the simulated thermal runaway test for fresh and cycled cells DME (green), DEG (red) and TEG (blue). (b,f) are enlarged views of (a,e). The heating rate is 5 K min^{-1}. (c,d), (g,h) First derivatives of the TJs for (c,g) DME-cells and (d,h) DEG-cells. (i-q) Digital photo of the DME, DEG and TEG cell before (i,l,o), fresh cells after simulated thermal runaway test (j,m,p) and after cycles cells after simulated thermal runaway test (k,n,q), respectively. (j,m) The six components after the test are presented in the order of glass fibre, Mg foil, Ni foam, top cap, cathode, bottom cap. Scanning electron microscopy images of the original states (Fig. 3r,t) and the 3rd cycled state after explosion (Fig. 3s,u). (For interpretation of the references to colour in this figure legend, the reader is referred to the web version of this article.)

components of the cell are all scattered in the testing chamber (Fig. 3j and Fig. S2a, Supporting Information). The DEG-cell remains largely intact but with a big crack, leading to the evaporation of all the DEG electrolyte (Fig. 3m and Fig. S2b, Supporting Information). The glass fibre separator layer is found to 'stretch' outside the cell. During the fast gasification, part of the glass fibre layer is carried outside the cell by the DEG electrolyte to release the over-pressure. Finally, the TEG-cell remains fully intact (Fig. 3p and Fig. S2c, Supporting Information) until reaching the temperature of the testing limit (523 K).

The first derivatives of both TJs show negative peaks in the DME and DEG-cells (Fig. 3c and d), indicating an endothermic process during explosion. This can be understood as the pure thermal expansion of the vaporized electrolyte during the explosion, which absorbs heat from the environment [44,45]. Therefore, the explosion of fresh DME and DEG cells is mainly a physical process due to the over-pressure caused by electrolyte vaporization and expansion.

Next, the sample explosion test was applied to the cells after three discharge and charge cycles. TJ is only recorded for the cycled-DME-cell, whereas those of the cycled-DEG-cell and cycled-TEG-cell show a steady temperature profile (Fig. 3f). This is also observed in the first derivatives

profiles, in which the cycled-DME-cell shows a positive peak (Fig. 3g) whereas the cycled-DEG-cell present a flat line (Fig. 3h). The positive peak here indicates an exothermic process for the cycled-DME-cell during explosion, which is different from its fresh state. This can be understood as the unstable decomposition reaction of the intermediate product MgS (Fig. S3, Supporting Information) after cycles, which reacts as $MgS + 2H_2O \rightarrow Mg(OH)_2 + H_2S$, $\Delta H = -133.5$ kJ mol^{-1}, releasing heat. Comparison of the SEM images of cathode in the original states (Fig. 3r) and the 3rd cycled state after explosion (Fig. 3s, and Fig. S4, Supporting Information) shows a slight aggregation of S particles. This is because of the dissolution and precipitation out of S during charging and discharging. On the anode side, no significant cracking or damage is observed in the Mg foil, except for the deposition of the glass fibres at the surface (Fig. 3t,u and Fig. S5, Supporting Information, which is likely due to cell disassembly). Though there were no significant fluctuation in the time-temperature curve for cycled-DEG-cell (Fig. S6a-d, Supporting Information), cracks were observed after the thermal runaway test. This indicates the leak of DEG during the heating (Fig. S6e, Supporting Information).

The explosion temperatures are 45 K and 20 K above the boiling points of DME and DEG (Fig. 3a and e), respectively. This may be caused by a thermal resistance from the chamber environment to the inner cell. To examine this, a range of heating rates from 1 K min^{-1} to 20 K min^{-1} are tested. Surprisingly, the explosion temperatures for DME and DEG stay constantly at 403 ± 4 K and 455 ± 6 K, respectively, regardless of the heating rate (Fig. 4a). The pressure of the cell is then calculated by using the vapour pressure equation and is plotted as the function of time (Fig. S7, Supporting Information). The calculated vapour pressures at the explosion temperature are 249 ± 14 kPa for DME and 172 ± 28 kPa for DEG, respectively (Fig. 4b). Sulfur does not contribute to the inner pressure built up, as the calculated sulfur vapour pressures at those conditions are 0.006 and 0.11 kPa, respectively. Because the electrolyte vapour is the main reason for the over-pressure in the cell, the calculated vapour pressure can also reflect the real inner pressure of the cell. If decomposition of the electrolyte takes place, an additional pressure is built up. This leads to further decrease of the thermal runaway temperature (Table S1 and Fig. S8, Supporting Information). The sealing pressure of the coin cell can also influence the explosion temperature. Raising the sealing pressure from 0.5 to 0.75 TON increases the thermal runaway temperature from 393 to 439 K (Fig. S9, Supporting Information) for DME-based electrolyte. The explosion temperature is then stabilized between 439 and 451 K when the sealing pressure further increases to 1.4 TONs. At 0.5 TON of the standard sealing condition, the DME-cell only explodes at 149 kPa over-pressure from the environment, while the DEG-cell explodes with 72 kPa over-pressure (albeit at different failure temperatures). This indicates the upper pressure limit of the CR2032 cell at 403 K and 455 K, respectively. The Nylon-6 O-ring that seals the cells becomes less thermally stable above 423 K [46]. Its ability to withhold the over-pressure then decreases. To verify this, the Nylon-6 O-ring was tested in the BTC under the same temperature programme. After testing, the Nylon-6 O-ring was completely melted (Fig. S10, Supporting Information). The influence of cathode sulfur loading to the explosion temperature is further studied, in order to examine if there can be any combustion of the sulfur. The result shows again the constant explosion temperature at 403 ± 4 K and 455 ± 6 K for DME and DEG-cells, respectively, regardless of the sulfur loading (Fig. 4c). DME was further mixed with DEG or TEG at the volume ratios of 3:1, 1:1 and 1:3, respectively, to form the mixed solvent systems. The thermal runaway temperature increases with the raising content of DEG or TEG (Fig. S11a-c, Supporting Information). The overall thermal runaway temperature shows a positive correlation with the average carbon atom per molecule in the mixed electrolyte, suggesting the causal relations between molecular structure and its explosion behaviour (Fig. S12, Supporting Information). The discharge/charge curves of various electrolytes show that the electrochemical performance of mixed electrolyte (DME+DEG or DME+TEG) mixture is between that of pure electrolyte systems (Fig. S11d). These phenomena further confirm that thermal runaway and electrochemical performance are closely tied to the chain length of the electrolyte. We further studied Magnesium bis (hexamethyldisilazide) $Mg(HMDS)_2$ as an organic non-nucleophilic electrolyte [47–49] (Fig. S13, Supporting Information). It is not soluble in DME but soluble in DEG and TEG. Similar to the thermal runaway test with $Mg(TFSI)_2$ electrolyte, a small TJ is found for DEG solvent at 438 K with 3 K min^{-1}, whereas the TEG cell does not explode.

With the measured specific capacity, the explosion temperature and indicatives prices of the three electrolytes in the Acros, a comprehensive diagram can be drawn to balance the performance, cost and safety of the Mg-S batteries (Fig. 5a). The DME-cell is clearly favoured by performance and cost, whereas the safety of DME requires serious consideration. In this regard, design of DME derivatives with higher boiling point and the same Mg^{2+} conductivity is suggested. The risk of combustion is high in DME-cells, in particular the practical pouch cells. The trends of performance, safety and cost are directly related to the number of repeating units in three $CH_3O(CH_2CH_2O)_nCH_3$ electrolytes (Fig. 5b). In general, longer chain length leads to 1) high boiling point, thus high explosion temperature; 2) high Mg^{2+} conduction resistance and low storage capacity; 3) long synthetic process and high separation cost.

3. Conclusions

In conclusion, a general approach that evaluates the performance, safety and cost of the electrolyte in Mg-S battery is developed. The combustion of the metal anode is not found in the Mg-S battery for all three electrolyte systems under the failure scenarios studied here, which provides a compelling improvement compared with other alkali metal anodes. The explosion temperature is positively correlated with the

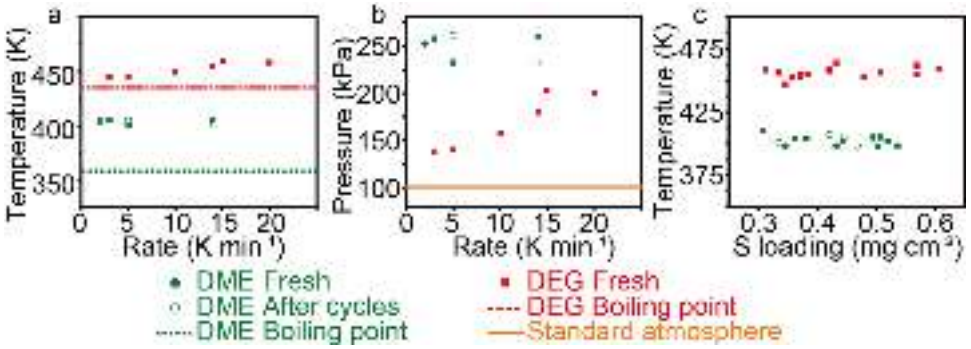

Fig. 4. (a) Explosion temperature as a function of heating rates for DME (green) and DEG-cells (red). (b) The corresponding vapour pressure at the explosion temperature. (c) Explosion temperature as the function of the sulfur loading for DME (green) and DEG-cells (red). The TEG cells does not explode due to the high boiling point of TEG. (For interpretation of the references to colour in this figure legend, the reader is referred to the web version of this article.)

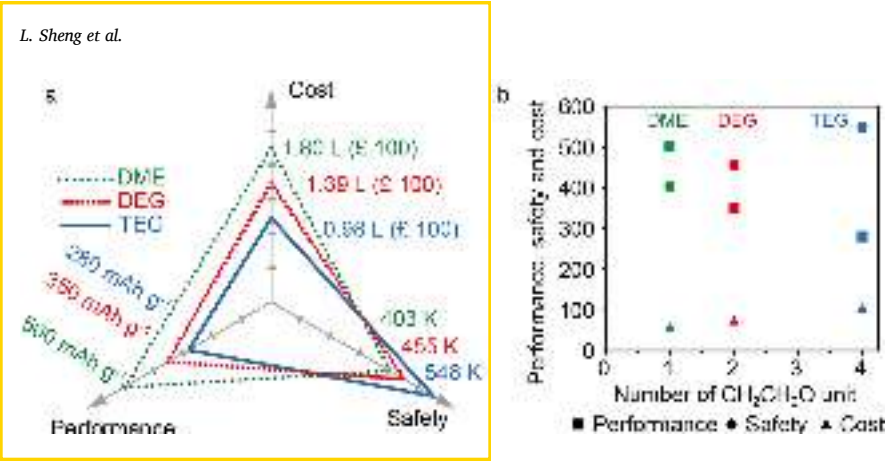

Fig. 5. (a) The discharge capacity (Performance), and the explosion temperature for DME (green), DEG (red) and TEG-cells (blue), and the quantity of electrolyte with the value £ 100. The explosion temperature of the DME and DEG cells are taken from the average values in Fig. 4. The explosion temperature of the TEG cell is estimated to be its boiling point. (b) The discharge capacity (mAh g^{-1}), explosion temperature (K) and listed price at Acros (£) per one litre as the function of n in $CH_3O(CH_2CH_2O)_nCH_3$. (For interpretation of the references to colour in this figure legend, the reader is referred to the web version of this article.)

electrolyte vapour pressures and boiling points, which are the key descriptor for the safety limits of Mg-S battery. The number of the repeating unit in the electrolyte plays a decisive role in the overall battery evaluations. In general, small chain ether based electrolytes with low boiling points have a low explosion temperature. In contrast, the Mg^{2+} mobility is higher in those small chain electrolytes, leading to a better charge and discharge performance. Therefore, a potential method to realize the improvement of battery safety, while at the same time maintaining or even improving the battery performance, is to design small chain molecules with higher molecular weight or polarity, thus obtaining a higher boiling point and low vapour pressure. It is also important to study the temperature distribution within the batteries to understand the origin of the explosion. As the Mg-S technology matures, the application of these methods to larger format cells will continue to provide useful insight to benchmark its safety of compared with other cell chemistries.

4. Experimental section

4.1. Battery testing calorimeter

Thermal runaway testing was conducted inside a Phi-Tec Battery Testing Calorimeter (BTC) (Fig. S1, Supporting Information). The coin cell is taped with the thermal couples to measure the temperature increase. The cell is placed into a protected explosion chamber. Temperature programmed heating is set at various fixed rates to reach 523 K. The temperature of the cell is measured every 5 s. After the test, the chamber is opened and the cell is examined. Each test is repeated at least three times.

4.2. Synthesis of CMK-3/S composites as cathode materials

The Mg-S battery tested in BTC uses a CMK-3/S composite as the cathode. CMK-3 is an ordered mesoporous carbon material with high surface area (1141 m^2 g^{-1}) and large pore volume (1.38 cm^3 g^{-1}) (Fig. S14, Supporting Information). In a typical experiment to produce CMK-3/S composite, 0.5 g of CMK-3 powder is physically mixed with 0.5 g of sulfur. The mixture is then transferred into a batch reactor under argon with subsequent heating at 428 K for 24 h. The sulfur melts and is impregnated into the pore network of CMK-3. The diffraction peaks in the X-ray diffraction pattern (XRD) are not obvious (Fig. S15, Supporting Information), suggesting the formation of quasi-amorphous S. The S is indeed impregnated into the CMK-3 channels, as uniform distribution of S and C is observed in the energy-dispersive X-ray spectroscopy (Fig. S16, Supporting Information).

4.3. Electrolyte preparation

Three types of electrolytes were chosen and prepared in an Ar filled glovebox by adding magnesium(II) bis(trifluoromethanesulfonyl)imide ($Mg(TFSI)_2$) into the DME, DEG and TEG, respectively. After three hours of stirring, magnesium chloride ($MgCl_2$) was added into the electrolytes and stirring overnight. The molar ratio of $Mg(TFSI)_2$ and $MgCl_2$ is 1: 0.8. The concentration of the Mg^{2+} is 1.8 mol L^{-1}.

Four types of electrolytes were prepared in an Ar filled glovebox by adding magnesium(II) bis(trifluoromethanesulfonyl)imide ($Mg(TFSI)_2$) into pure DOL and DOL/DME mixed solvent with volume ratios of 1:3, 1:1 and 3:1. After stirring for 3 h, magnesium chloride ($MgCl_2$) was added into the electrolytes and stirred overnight. The molar ratio of $Mg(TFSI)_2$ to $MgCl_2$ was 1: 0.8, and the Mg^{2+} concentration was 1.8 mol L^{-1}.

Two types of electrolytes ($Mg(HMDS)_2$ system) were prepared in an Ar filled glovebox. 1.24 g (3.6 mmol) $Mg(HMDS)_2$ was dissolved in 4 ml DEG or TEG in a vial, then 0.96 g (7.2 mmol) $AlCl_3$ was slowly added and stirred for 24 h at room temperature. Subsequently about 0.343 g (3.6 mmol) $MgCl_2$ was added portionwise to the solution and stirred for 40 h.

4.4. Electrochemical measurements

All the electrochemical measurements were tested with CR2032 coin cells with magnesium foil from Goodfellow as anode, previously prepared electrolyte, Whatman glass fiber as separator and CMK-3/S cathode. This cathode was fabricated by mixing CMK-3/S composite, super P, sodium carboxyl methyl cellulose (NaCMC) and styrene butadiene rubber (SBR) in a weight ratio of 80: 10: 5: 5 in deionized water. The slurry was coated on carbon coated aluminium foil and dried at 60 °C overnight in vacuum oven. Then, the electrode was roll pressed, and punched into round discs of 6 mm in diameter with mass loading from 0.3 to 0.6 mg_{sulfur} cm^{-2}. The volume of electrolyte is 150 μL for all the cells. Galvanostatic charge and discharge were tested in a voltage window of 0.4–1.8 V on a battery measurement system (Neware).

4.5. Characterization and thermal runaway test

XRD measurements were performed using a StadiP diffractometer from STOE, a voltage of 40 kV, at 30 mA, with Cu Kα radiation, scan in the 2θ range between 0° and 90° at a rate of 6° min^{-1} with step size of 0.5°. Nitrogen adsorption–desorption isotherms were recorded at 77 K using a Micromeritics 3Flex surface characterization analyzer. Specific surface areas were determined according to the BET model, with pore diameters, volumes, and distributions determined through the BJH method. Scanning transmission electron microscopy (STEM) study was performed using a probe corrected (CEOS) JEM ARM 200CF (JEOL, Japan) operated at 200 kV. Bright Field (BF) and High Angle Annular Dark Field (HAADF) images were acquired simultaneously. EDS elemental mapping was performed on the same microscope. Scanning electron microscopy (SEM) imaging and related element mapping were performed on a JEOL JSM-7401F SEM.

CRediT authorship contribution statement

Lin Sheng: Performs most experiment, prepare original manuscript. **Zhangxiang Hao:** Contributes main idea, performs some experiment and co-write paper. **Junrun Feng, Wenjia Du, Manxi Gong, Liqun Kang:** Help to do some experiment and characterization. **Paul R. Shearing, Dan J. L. Brett:** Provide the equipment and discuss the results. **Yunhui Huang:** Provides the equipment, contributes the proposal and corrects the paper. **Feng Ryan Wang:** Provides the equipment, contributes the proposal and corrects the paper.

Declaration of Competing Interest

The authors declare that they have no known competing financial interests or personal relationships that could have appeared to influence the work reported in this paper.

Acknowledgement

Lin Sheng and Zhangxiang Hao contributed equally to this work. The project is funded by EPSRC (EP/P02467X/1 and EP/S018204/1), Royal Society (RG160661, IES\R3\170097) and the Centre for Nature Inspired Chemical Engineering (EP K038656/1). We acknowledge the electron Physical Science and Imaging Centre (ePSIC) and Diamond Light Source (DLS) for the allocated STEM experiment session (Proposal No. EM20643). Lin Sheng thanks the China Scholarship Council (201908060125) (CSC) for the Ph.D. funding. Paul R. Shearing acknowledges funding from The Royal Academy of Engineering (CiET1718/59) and The Faraday Institution (EP/S003053/1, FIRG0014).

Appendix A. Supporting information

Supplementary data associated with this article can be found in the online version at doi:10.1016/j.nanoen.2021.105832.

References

[1] B. Dunn, H. Kamath, J.M. Tarascon, Electrical energy storage for the grid: a battery of choices, Science 334 (2011) 928–935, https://doi.org/10.1126/science.1212741.
[2] J.M. Tarascon, M. Armand, Issues and challenges facing rechargeable lithium batteries, Nature 414 (2001) 359–367, https://doi.org/10.1038/35104644.
[3] J.B. Goodenough, Y. Kim, Challenges for rechargeable Li batteries, Chem. Mater. 22 (2010) 587–603, https://doi.org/10.1021/cm901452z.
[4] C. Liu, F. Li, M. Lai-Peng, H.M. Cheng, Advanced materials for energy storage, Adv. Mater. 22 (2010) E28–E62, https://doi.org/10.1002/adma.200903328.
[5] H.D. Yoo, E. Markevich, G. Salitra, D. Sharon, D. Aurbach, On the challenge of developing advanced technologies for electrochemical energy storage and conversion, Mater. Today 17 (2014) 110–121, https://doi.org/10.1016/j.mattod.2014.02.014.
[6] Y. Wang, R. Chen, T. Chen, H. Lv, G. Zhu, L. Ma, C. Wang, Z. Jin, J. Liu, Emerging non-lithium ion batteries, Energy Storage Mater. 4 (2016) 103–129, https://doi.org/10.1016/j.ensm.2016.04.001.
[7] F. Wu, G. Yushin, Conversion cathodes for rechargeable lithium and lithium-ion batteries, Energy Environ. Sci. 10 (2017) 435–459, https://doi.org/10.1039/c6ee02326f.
[8] N.S. Choi, Z. Chen, S.A. Freunberger, X. Ji, Y.K. Sun, K. Amine, G. Yushin, L. F. Nazar, J. Cho, P.G. Bruce, Challenges facing lithium batteries and electrical double-layer capacitors, Angew. Chem. Int. Ed. 51 (2012) 9994–10024, https://doi.org/10.1002/anie.201201429.
[9] A. Manthiram, Materials challenges and opportunities of lithium ion batteries, J. Phys. Chem. Lett. 2 (2011) 176–184, https://doi.org/10.1021/jz1015422.
[10] X. Hong, J. Mei, L. Wen, Y. Tong, A.J. Vasileff, L. Wang, J. Liang, Z. Sun, S.X. Dou, Nonlithium metal–sulfur batteries: steps toward a leap, Adv. Mater. 31 (2019), 1802822, https://doi.org/10.1002/adma.201802822.
[11] R. Mohtadi, F. Mizuno, Magnesium batteries: current state of the art, issues and future perspectives, Beilstein J. Nanotechnol. 5 (2014) 1291–1311, https://doi.org/10.3762/bjnano.5.143.
[12] C.B. Bucur, T. Gregory, A.G. Oliver, J. Muldoon, Confession of a magnesium battery, J. Phys. Chem. Lett. 6 (2015) 3578–3591, https://doi.org/10.1021/acs.jpclett.5b01219.
[13] X. Zhou, J. Tian, J. Hu, C. Li, High rate magnesium–sulfur battery with improved cyclability based on metal–organic framework derivative carbon host, Adv. Mater. 30 (2018), 1704166, https://doi.org/10.1002/adma.201704166.
[14] S.Y. Ha, Y.W. Lee, S.W. Woo, B. Koo, J.S. Kim, J. Cho, K.T. Lee, N.S. Choi, Magnesium(II) bis(trifluoromethane sulfonyl) imide-based electrolytes with wide electrochemical windows for rechargeable magnesium batteries, ACS Appl. Mater. Interfaces 6 (2014) 4063–4073, https://doi.org/10.1021/am405619v.
[15] X.C. Hu, Y. Shi, S.Y. Lang, X. Zhang, L. Gu, Y.G. Guo, R. Wen, L.J. Wan, Direct insights into the electrochemical processes at anode/electrolyte interfaces in magnesium-sulfur batteries, Nano Energy 49 (2018) 453–459, https://doi.org/10.1016/j.nanoen.2018.04.066.
[16] Y. Xu, W. Li, G. Zhou, Z. Pan, Y. Zhang, A non-nucleophilic mono-Mg^{2+} electrolyte for rechargeable Mg/S battery, Energy Storage Mater. 14 (2018) 253–257, https://doi.org/10.1016/j.ensm.2018.03.020.
[17] R. Davidson, A. Verma, D. Santos, F. Hao, C. Fincher, S. Xiang, J. Van Buskirk, K. Xie, M. Pharr, P.P. Mukherjee, S. Banerjee, Formation of magnesium dendrites during electrodeposition, ACS Energy Lett. 4 (2019) 375–376, https://doi.org/10.1021/acsenergylett.8b02470.
[18] P. Wang, M.R. Buchmeiser, Rechargeable magnesium–sulfur battery technology: state of the art and key challenges, Adv. Funct. Mater. 29 (2019), 1905248, https://doi.org/10.1002/adfm.201905248.
[19] P. Saha, P.H. Jampani, D.H. Hong, B. Gattu, J.A. Poston, A. Manivannan, M. K. Datta, P.N. Kumta, Synthesis and electrochemical study of $Mg_{1.5}MnO_3$: a defect spinel cathode for rechargeable magnesium battery, Mater. Sci. Eng. B Solid State Mater. Adv. Technol. 202 (2015) 8–14, https://doi.org/10.1016/j.mseb.2015.08.008.
[20] L. Kong, C. Yan, J.-Q. Huang, M.-Q. Zhao, M.-M. Titirici, R. Xiang, Q. Zhang, A review of advanced energy materials for magnesium-sulfur batteries, Energy Environ. Mater. 1 (2018) 100–112, https://doi.org/10.1002/eem2.12012.
[21] Z. Zhao-Karger, M. Fichtner, Magnesium-sulfur battery: its beginning and recent progress, MRS Commun. 7 (2017) 770–784, https://doi.org/10.1557/mrc.2017.101.
[22] S.H. Chung, A. Manthiram, Current status and future prospects of metal–sulfur batteries, Adv. Mater. 31 (2019), 1901125, https://doi.org/10.1002/adma.201901125.
[23] Z. Zhao-Karger, M.E. Gil Bardaji, O. Fuhr, M. Fichtner, A new class of non-corrosive, highly efficient electrolytes for rechargeable magnesium batteries, J. Mater. Chem. A 5 (2017) 10815–10820, https://doi.org/10.1039/c7ta02237a.
[24] T. Gao, M. Noked, A.J. Pearse, E. Gillette, X. Fan, Y. Zhu, C. Luo, L. Suo, M. A. Schroeder, K. Xu, S.B. Lee, G.W. Rubloff, C. Wang, Enhancing the reversibility of Mg/S battery chemistry through Li^+ mediation, J. Am. Chem. Soc. 137 (2015) 12388–12393, https://doi.org/10.1021/jacs.5b07820.
[25] B.P. Vinayan, Z. Zhao-Karger, T. Diemant, V.S.K. Chakravadhanula, N. I. Schwarzburger, M.A. Cambaz, R.J. Behm, C. Kübel, M. Fichtner, Performance study of magnesium-sulfur battery using a graphene based sulfur composite cathode electrode and a non-nucleophilic Mg electrolyte, Nanoscale 8 (2016) 3296–3306, https://doi.org/10.1039/c5nr04383b.
[26] T. Gao, S. Hou, F. Wang, Z. Ma, X. Li, K. Xu, C. Wang, Reversible S0/MgS_x redox chemistry in a $MgTFSI_2$/$MgCl_2$/DME electrolyte for rechargeable Mg/S batteries, Angew. Chem. Int. Ed. 56 (2017) 13526–13530, https://doi.org/10.1002/anie.201708241.
[27] K. Kitoh, H. Nemoto, 100 Wh large size Li-ion batteries and safety tests, J. Power Sources 81–82 (1999) 887–890, https://doi.org/10.1016/S0378-7753(99)00125-1.
[28] R. Kizilel, R. Sabbah, J.R. Selman, S. Al-Hallaj, An alternative cooling system to enhance the safety of Li-ion battery packs, J. Power Sources 194 (2009) 1105–1112, https://doi.org/10.1016/j.jpowsour.2009.06.074.
[29] D. Doughty, E.P. Roth, A general discussion of Li Ion battery safety, Electrochem. Soc. Interface 21 (2012) 37–44, https://doi.org/10.1149/2.F03122if.
[30] E.P. Roth, C.J. Orendorff, How electrolytes influence battery safety, Electrochem. Soc. Interface 21 (2012) 45–49, https://doi.org/10.1149/2.F04122if.
[31] K. Liu, Y. Liu, D. Lin, A. Pei, Y. Cui, Materials for lithium-ion battery safety, Sci. Adv. 4 (2018), eaas9820, https://doi.org/10.1126/sciadv.aas9820.
[32] D.P. Finegan, J. Darst, W. Walker, Q. Li, C. Yang, R. Jervis, T.M.M. Heenan, J. Hack, J.C. Thomas, A. Rack, D.J.L. Brett, P.R. Shearing, M. Keyser, E. Darcy, Modelling and experiments to identify high-risk failure scenarios for testing the safety of lithium-ion cells, J. Power Sources 417 (2019) 29–41, https://doi.org/10.1016/j.jpowsour.2019.01.077.
[33] Q. Wang, L. Jiang, Y. Yu, J. Sun, Progress of enhancing the safety of lithium ion battery from the electrolyte aspect, Nano Energy 55 (2019) 93–114, https://doi.org/10.1016/j.nanoen.2018.10.035.
[34] G. Zhang, L. Cao, S. Ge, C.Y. Wang, C.E. Shaffer, C.D. Rahn, Reaction temperature sensing (RTS)-based control for Li-ion battery safety, Sci. Rep. 5 (2015), 18237, https://doi.org/10.1038/srep18237.
[35] R. Chen, A.M. Nolan, J. Lu, J. Wang, X. Yu, Y. Mo, L. Chen, X. Huang, H. Li, The thermal stability of lithium solid electrolytes with metallic lithium, Joule 4 (2020) 812–821, https://doi.org/10.1016/j.joule.2020.03.012.
[36] T.M. Bandhauer, S. Garimella, T.F. Fuller, A critical review of thermal issues in lithium-ion batteries, J. Electrochem. Soc. 158 (2011), R1, https://doi.org/10.1149/1.3515880.
[37] Q. Wang, P. Ping, X. Zhao, G. Chu, J. Sun, C. Chen, Thermal runaway caused fire and explosion of lithium ion battery, J. Power Sources 208 (2012) 210–224, https://doi.org/10.1016/j.jpowsour.2012.02.038.
[38] J. Duan, X. Tang, H. Dai, Y. Yang, W. Wu, X. Wei, Y. Huang, Building safe lithium-ion batteries for electric vehicles: a review, Electrochem. Energy Rev. 3 (2020) 1–42, https://doi.org/10.1007/s41918-019-00060-4.

[39] G. Xu, L. Huang, C. Lu, X. Zhou, G. Cui, Revealing the multilevel thermal safety of lithium batteries, Energy Storage Mater. 31 (2020) 72–86, https://doi.org/10.1016/j.ensm.2020.06.004.
[40] L. Carbone, M. Gobet, J. Peng, M. Devany, B. Scrosati, S. Greenbaum, J. Hassoun, Comparative study of ether-based electrolytes for application in lithium-sulfur battery, ACS Appl. Mater. Interfaces 7 (2015) 13859–13865, https://doi.org/10.1021/acsami.5b02160.
[41] X. Feng, J. Sun, M. Ouyang, F. Wang, X. He, L. Lu, H. Peng, Characterization of penetration induced thermal runaway propagation process within a large format lithium ion battery module, J. Power Sources 275 (2015) 261–273, https://doi.org/10.1016/j.jpowsour.2014.11.017.
[42] A.W. Golubkov, D. Fuchs, J. Wagner, H. Wiltsche, C. Stangl, G. Fauler, G. Voitic, A. Thaler, V. Hacker, Thermal-runaway experiments on consumer Li-ion batteries with metal-oxide and olivin-type cathodes, RSC Adv. 4 (2014) 3633–3642, https://doi.org/10.1039/c3ra45748f.
[43] S. Wilke, B. Schweitzer, S. Khateeb, S. Al-Hallaj, Preventing thermal runaway propagation in lithium ion battery packs using a phase change composite material: an experimental study, J. Power Sources 340 (2017) 51–59, https://doi.org/10.1016/j.jpowsour.2016.11.018.
[44] X. Ge, X. Wang, Estimation of freezing point depression, boiling point elevation, and vaporization enthalpies of electrolyte solutions, Ind. Eng. Chem. Res. 48 (2009) 2229–2235, https://doi.org/10.1021/ie801348c.
[45] V.S. Patwardhan, A. Kumar, A unified approach for prediction of thermodynamic properties of aqueous mixed-electrolyte solutions part I: vapor pressure and heat of vaporization, AIChE J. 32 (1986) 1419–1428, https://doi.org/10.1002/aic.690320903.
[46] G. Rusu, E. Rusu, Evaluation of thermal and dielectric behaviour of some anionic nylon 612 copolymers, Mater. Des. 31 (2010) 4601–4610, https://doi.org/10.1016/j.matdes.2010.05.042.
[47] Z. Zhao-Karger, X. Zhao, D. Wang, T. Diemant, R.J. Behm, M. Fichtner, Performance improvement of magnesium sulfur batteries with modified non-nucleophilic electrolytes, Adv. Energy Mater. 5 (2015), 1401155, https://doi.org/10.1002/aenm.201401155.
[48] A. Du, Z. Zhang, H. Qu, Z. Cui, L. Qiao, L. Wang, J. Chai, T. Lu, S. Dong, T. Dong, H. Xu, X. Zhou, G. Cui, An efficient organic magnesium borate-based electrolyte with non-nucleophilic characteristics for magnesium-sulfur battery, Energy Environ. Sci. 10 (2017) 2616–2625, https://doi.org/10.1039/c7ee02304a.
[49] D. Huang, S. Tan, M. Li, D. Wang, C. Han, Q. An, L. Mai, Highly efficient non-nucleophilic $Mg(CF_3SO_3)_2$-based electrolyte for high-power Mg/S battery, ACS Appl. Mater. Interfaces 12 (2020) 17474–17480, https://doi.org/10.1021/acsami.0c00196.

Ms. Lin Sheng received her Msc degree from East China University of Technology. From 2018, she works as a PhD candidate in the University College London (UCL). Her current research focuses on Mg-S battery, solid-state battery and electrodes for Lithium-ion battery.

Dr. Zhangxiang Hao received his PhD degree from Huazhong University of Science and Technology (HUST). From 2018, he works as a postdoctoral researcher in the University College London (UCL). His current research focuses on rechargeable Li-S battery, Mg-S battery and solid-state battery.

Mr. Junrun Feng received his MSc degree from University College London (UCL). From 2018, he works as a PhD candidate in chemical engineering department of UCL. His current research focuses on All solid-state battery, electrodes for Lithium-ion battery and Mg-S battery.

Dr. Wenjia Du is a research fellow at electrochemical innovation lab (EIL), University College London. He obtained his PhD at University of Hull, UK in 2018. His research focuses on *in-situ* studying a wider range of materials (from metals to Li-S batteries) using multiscale X-ray imaging techniques both at laboratory or synchrotron sources.

Ms. Manxi Gong got MSc degree in materials for energy and environment from University College London (UCL). From 2020, she works as a PhD candidate in the chemical engineering department of UCL. Her current research focuses on nano-catalysts in electrochemistry synchrotron-based X-ray techniques for material characterization.

Mr. Liqun Kang holds a BSc degree in chemistry from Peking University (PKU) and he is a PhD candidate in chemical engineering at University College London (UCL). His research focuses on development of single-atomic-site catalysts, which embraces controlled material synthesis and advanced synchrotron-based X-ray techniques for material characterisation.

Dr. Paul Shearing is a Professor in Chemical Engineering at University College London where he holds The Royal Academy of Engineering Chair in Emerging Battery Technologies. His research interests cover a broad range of electrochemical engineering themes with a particular interest in the relationship between performance and microstructure for energy materials. He co-directs UCL's Electrochemical Innovation lab and leads the UK STFC Global Challenge Network in Batteries and Electrochemical Devices. He was a founding investigator of the UK's Faraday Institution, where he chairs the Training & Diversity Panel and is PI of the LiSTAR programme investigating Li-sulfur battery technologies.

Dr. Yunhui Huang received his BSc, MSc and PhD from Peking University. In 2000, he worked as a postdoctoral researcher in Peking University. From 2002–2004, he worked as an associate professor in Fudan University and a JSPS fellow at Tokyo Institute of Technology, Japan. He then worked with Prof. John B. Goodenough in the University of Texas at Austin from 2004 to 2007. In 2008, he became a chair professor of materials science in Huazhong University of Science and Technology. His research group works on batteries of energy storage and conversion.

Dr. Feng Ryan Wang received his PhD degree from Peking University in 2012. He was an Alexander *von* Humboldt post-doctoral fellow at Max-Planck-Institute für Kohlenforschung between 2012 and 2015. He joined University College London (UCL) in 2016 and led the Materials and Catalysis Laboratory (MCL). His group works in the study of materials structural dynamics under working conditions using a range of *operando* techniques.